This article has been accepted for inclusion in a future issue of this journal. Content is final as presented, with the exception of pagination.

Filtered Split-Path Nonlinear Integrator: A Hybrid Controller for Transient Performance Improvement

B. Sharif, A. van der Maas, N. van de Wouw, *Fellow, IEEE*, and W. P. M. H. Heemels, *Fellow, IEEE*

***Abstract*— The filtered split-path nonlinear integrator (F-SPANI) is a generic nonlinear controller designed to improve the transient performance of linear (motion) systems in terms of overshoot. The main idea underlying F-SPANI is that the amplitude and phase of an integrator can be tuned using independent filters, resulting in more efficient use of the buffer of the integrator. In this article, a general description of F-SPANI is presented. In addition, a stability analysis result is presented that provides sufficient conditions in the form of linear matrix inequalities (LMIs) for closed-loop stability analysis on the basis of construction of a common quadratic Lyapunov function (CQLF). The ease of the design, implementation, and the potential of the proposed controller are illustrated both in simulations and in experiments on an industrial pick-and-place machine.**

***Index Terms*— Hybrid control, motion control, stability analysis, transient performance.**

I. Introduction

CLASSICAL linear control theory suffers from fundamental limitations, such as the waterbed effect due to the Bode sensitivity integral and the Bode gain-phase relationship (see [1], [2]). In linear time-invariant (LTI) feedback control, this limitation results in a tradeoff between a desirable transient performance and low-frequency disturbance suppression [3]. A linear integrator is a typical example in feedback control, where a tradeoff is made between a zero steady-state tracking error at the cost of introducing (additional) overshoot due to the 90° phase lag of the integrator, i.e., disturbance suppression at the cost of transient performance.

Over the years, several nonlinear and hybrid control strategies have been proposed to improve the transient performance of LTI systems [4], by overcoming this fundamental limitation of LTI control techniques. The Clegg integrator [5] is an example of a reset controller where (a subset of) the internal controller states are reset according to some decision criterion to reduce the overshoot. This class of reset controllers has regained interest over the past two decades, both in research [6]–[8] and industry [9]. Variable-gain integrators [10], [11], sliding mode controllers with saturated integrators [12] and hybrid integrator-gain systems [13], [14], are other examples of nonlinear/hybrid controllers designed to improve the transient performance of a system, specifically the overshoot, without reducing the disturbance suppression capability.

In this article, we are interested in a class of nonlinear controllers with roots in the split-path nonlinear (SPAN) filter, which was introduced in [15] and facilitates independent tuning of the phase and the amplitude characteristics. In [16], the so-called split-path nonlinear integrator (SPANI) is proposed by including an integrator in the SPAN filter. The main benefit of the SPANI in [16] is the combination of an increased transient performance compared to a linear integrator design and the ease of verifying the stability of the switching closed-loop system. Note in this respect that the SPANI design aims for an improved integrator design, with all the benefits of a linear integrator in terms of zero steady-state tracking error, but without the phase lag introduced by the $-90°$ phase of a linear integrator. The SPANI is easily tunable using standard tools for controller design based on, for instance, loop-shaping, thereby enabling straightforward adoption in industrial practice. In fact, without complex optimizations, the transient performance can be improved significantly. Verification of the stability of the SPANI is based on a linear matrix inequality (LMI) condition, which can easily be checked in an automated manner. The SPANI switches the sign of the integrator depending on the sign of the tracking error of the feedback loop. Since the system is in equilibrium for a zero error, it was observed that any slight disturbance will cause the controller to switch. To avoid the undesirable switching at the setpoint, the switching rule was adapted in [16] to include the equilibrium in the interior of the region corresponding to one of the modes of the switched system. This adapted switching rule results in additional undesirable phase lag. As a result, this adapted design of the SPANI does not reach the full potential for performance improvement since the phase lag results in delayed switching compared to the original SPANI, which in turn induces a larger overshoot. Hence, both SPANI designs in [16] have drawbacks that need to be overcome.

Manuscript received November 22, 2019; revised March 6, 2020 and November 23, 2020; accepted December 7, 2020. Manuscript received in final form January 5, 2021. This work was supported in part by the Netherlands Organisation for Scientific Research (NWO) through the CHAMeleon Research Programme (Hybrid Solutions for cost-Aware High-Performance Motion Control) under Project 13896. Recommended by Associate Editor K. Barton. *(Corresponding author: W. P. M. H. Heemels.)*

B. Sharif, A. van der Maas, and W. P. M. H. Heemels are with the Control Systems Technology Group, Department of Mechanical Engineering, Eindhoven University of Technology, 5600 MB Eindhoven, The Netherlands (e-mail: b.sharif@tue.nl; a.v.d.maas@tue.nl; m.heemels@tue.nl).

N. van de Wouw is with the Department of Mechanical Engineering, Eindhoven University of Technology, 5600 MB Eindhoven, The Netherlands, also with the Department of Civil, Environmental and Geo-Engineering, University of Minnesota, Minneapolis, MN 55455 USA, and also with the Delft Center for Systems and Control, Delft University of Technology, 2628 CD Delft, The Netherlands (e-mail: n.v.d.wouw@tue.nl).

Color versions of one or more figures in this article are available at https://doi.org/10.1109/TCST.2021.3050001.

Digital Object Identifier 10.1109/TCST.2021.3050001

1063-6536 © 2021 IEEE. Personal use is permitted, but republication/redistribution requires IEEE permission.
See https://www.ieee.org/publications/rights/index.html for more information.

Authorized licensed use limited to: Eindhoven University of Technology. Downloaded on May 02,2021 at 14:18:11 UTC from IEEE Xplore. Restrictions apply.

This article has been accepted for inclusion in a future issue of this journal. Content is final as presented, with the exception of pagination.

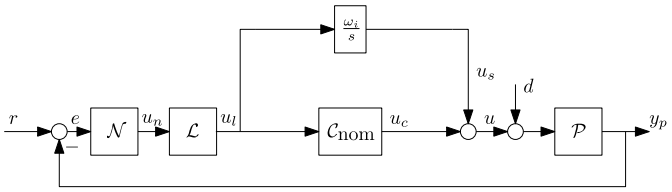

Fig. 1. Typical closed-loop control system.

The objective of this article is to indeed overcome the conservatism in the SPANI in terms of its transient performance by introducing a filtered split-path nonlinear integrator (F-SPANI) as a novel hybrid controller. The F-SPANI extends the SPANI structure by introducing a well-designed filter in the phase path. It is shown that the addition of a filter providing a phase lead, such as a lead filter, results in a significant improvement in closed-loop transient performance. The potential benefits of the novel F-SPANI design are shown in simulations. In addition, experiments on an industrial motion system are carried out in the context of pick-and-place applications, thereby illustrating next to the performance improvement also the ease of its design in the scope of an industrial high-tech application. Note that the experimental results involve a comparative study between a linear integrator design, the SPANI [16], and the proposed F-SPANI, which are novel for both the SPANI and the F-SPANI. Compared to our preliminary work [17] in which the F-SPANI was mentioned for the first time (only using a lead filter in the phase path), here we provide a general description of the system, including a complete stability analysis, of which the full proof is provided. In addition, an intuitive insight in the linear approximation of the nonlinear SPANI and F-SPANI is provided in terms of a describing function analysis next to new insights and experimental validation of both SPANI and F-SPANI on industrial equipment for pick-and-place applications.

The remainder of this article is organized as follows. In Section II, the hybrid control design is introduced. In Section III, the closed-loop properties of the F-SPANI are analyzed more thoroughly, starting with the stability analysis in Section III-B, followed by a describing function analysis of the controller in Section III-C. In Section III-D, a numerical example is shown to emphasize the potential benefits of the F-SPANI over the SPANI and the linear integrator. In Section IV, the experimental validation is provided. In Section V, the conclusions and recommendations of this article are presented.

II. Hybrid Control Setup

In this section, the hybrid controller setup is described in detail. In particular, this section will start with a problem statement in Section II-A, followed by the controller design in Section II-B.

A. Control Problem Statement

An integrator is a good example of a linear control element subject to a performance tradeoff. Typically, an integrator

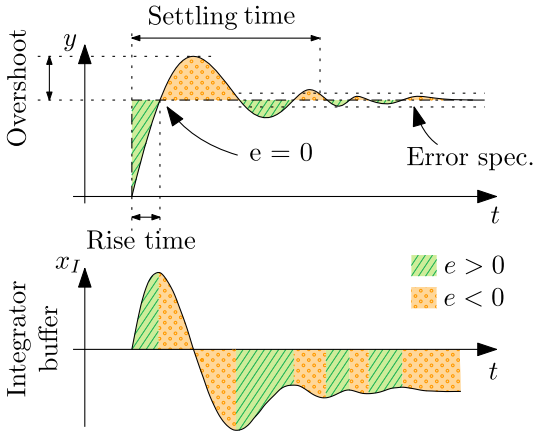

Fig. 2. Transient performance with integrator action.

is used to ensure a zero steady-state tracking error in the presence of (constant) disturbances. However, it results in overshoot and, therefore, a decreased transient performance. To understand this phenomenon, let us consider a typical closed-loop control scheme as shown in Fig. 1, where $\mathcal{N}$ represents a notch filter, $\mathcal{L}$ represents a low-pass filter, $\mathcal{C}_{\text{nom}}$ represents the nominal control loop without integrator, notch, and low pass, ω_i/s represents the integrator, and $\mathcal{P}$ represents the plant. The cause for the presence of overshoot in the system's response lies in the fact that the integrator builds up a buffer of the integrated error in the time domain, i.e., it "sums" error over time and stores it in its state. In particular, when a step reference is applied to such a system, the integral buffer builds up throughout the time of rise. At the moment when the sign of the error changes, the buffer still enforces an integrator action directed away from the reference as it is not emptied yet (the integrator still has the summed error stored in its state [6]). A schematic is given in Fig. 2. The green dashed surfaces depict areas where the error $e = r - y$ is positive, whereas the orange dotted surfaces depict areas where the error is negative. The surface actually represents the buffer of the integrator, which, as can be seen in the bottom half of the graph, does not change sign when the error does. The delayed behavior of the integral buffer is due to the $-90°$ phase of the integrator.

The phase lag between the sign change of the error and the sign change of the buffer of the integrator can be explained by the Bode-gain-phase relation by studying the frequency-domain representation of an integrator. A single integrator has a slope of -1 in the magnitude, i.e., -20 dB per decade, and a phase of $-90°$ for all frequencies. This phase lag explains why the integrator is lagging behind on the reference trajectory. An "ideal integrator" would have the advantage of the -1 slope in terms of the zero steady-state tracking error, however, it would not suffer from the phase lag due to the $-90°$ phase.

Due to the phase lag of an integrator, it is impossible for a linear system with integral action to achieve a step response without suffering from overshoot. The aim of this article is to design a hybrid controller with integral action that achieves the following:

Authorized licensed use limited to: Eindhoven University of Technology. Downloaded on May 02,2021 at 14:18:11 UTC from IEEE Xplore. Restrictions apply.

This article has been accepted for inclusion in a future issue of this journal. Content is final as presented, with the exception of pagination.

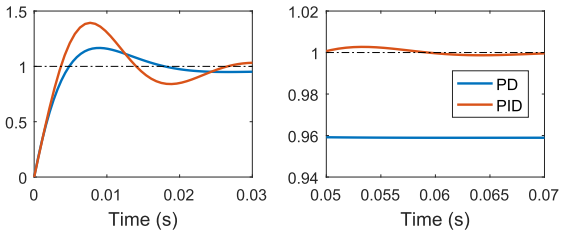

Fig. 3. Tradeoff between PD and PID control.

1) zero steady-state tracking error, achievable by using an integrator as indicated in the right of Fig. 3;
2) reduced *"phase lag"*;
3) and improved transient performance in terms of overshoot (and possibly settling time).

These improvements are all relative to the performance of the linear controller, designed using traditional loop-shaping techniques [3].

Remark 1: As an alternative to integral control, precompensation can be utilized in order to reduce the steady-state tracking error. In particular, by taking the precompensator as the inverse of the closed-loop dc gain, perfect tracking of constant disturbances can be achieved.

B. F-SPANI: Controller Design

In this section, a hybrid control strategy, called the F-SPANI and inspired by the SPANI [16], is proposed to improve the transient performance of a system compared to a corresponding linear controller. To arrive at the description of the novel F-SPANI controller, we first describe the original SPAN filter as introduced in [15]. Next, we extend the description to the SPANI filter in [16] and finally introduce the generic F-SPANI controller, which includes the SPANI as a special case. A description of the F-SPANI included in a typical feedback loop, as shown in Fig. 1, is described in Section III.

1) SPAN—Splitting the Phase and the Amplitude: The methods discussed in this section are based on the SPAN filter [15]. The general idea behind the SPAN filter is to independently tune the phase and the amplitude of a signal. This idea is in violation of the Bode gain-phase relationship, which does not hold for nonlinear or unstable systems. In Fig. 4, a schematic overview of the SPAN filter is given. In Fig. 4, $\mathcal{H}_1$ and $\mathcal{H}_2$ represent the filters for the amplitude and phase branches, respectively. The output v_1 of the amplitude filter $\mathcal{H}_1$ is fed to an absolute value element which retains all the magnitude information and removes all sign information, i.e., it outputs $|v_1|$. The output v_2 of $\mathcal{H}_2$ together with v_1 are fed to a sign element, which removes the amplitude information and retains all sign information (it outputs ± 1 depending on the sign of $v_1 v_2$). As a result of this construction, the output of the SPAN filter is

$$u_s = \begin{cases} v_1, & \text{if } v_1 v_2 > 0 \\ -v_1, & \text{if } v_1 v_2 < 0. \end{cases} \tag{1}$$

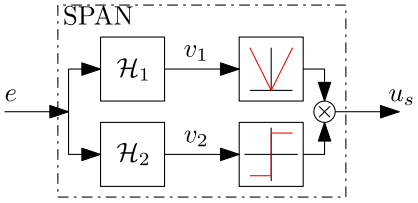

Fig. 4. SPAN filter.

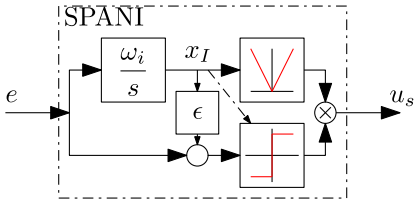

Fig. 5. SPANI filter.

As a result, it can be observed that $\mathcal{H}_1$ fully shapes the amplitude of the output signal u_s, whereas $\mathcal{H}_2$ shapes the phase of the output, i.e., either 0° or 180°.

2) SPANI: The SPANI from [16] is based on the SPAN filter, where

$$\mathcal{H}_1 = \mathcal{C}_I, \quad \mathcal{H}_2 = 1 \tag{2}$$

with $\mathcal{C}_I$ an integrator (see Fig. 5). In Fig. 5, ϵ is a nonnegative parameter, which will be discussed in more detail. In the following, we first assume that $\epsilon = 0$ to explain the rationale underlying the SPANI filter.

By using only the amplitude of the integrator and linking this to the sign of the error, the buffer of the integrator can be used to improve the transient performance. In particular, the sign function in the lower branch of Fig. 5 is defined as

$$\text{sign}(e, x_I) = \begin{cases} 1, & \text{if } e > 0 \\ 1, & \text{if } e = 0 \text{ and } x_I > 0 \\ -1, & \text{if } e = 0 \text{ and } x_I < 0 \\ -1, & \text{if } e < 0. \end{cases} \tag{3}$$

The buffer x_I of the integrator builds up, as shown in Fig. 2 by the green dashed surface in the initial part. At the point where $e = 0$, the buffer of the integrator has a positive value (see the bottom part of Fig. 2), which in turn creates a positive plant input, increasing the overshoot. By using the integrator part of the SPANI in the phase branch (see Fig. 5), the sign of the buffer is made equal to the sign of the error (see (3)), resulting in an integral action acting toward zero tracking error.

A few comments on the parameter ϵ are now in order. When $\epsilon > 0$, the switching of u_s in relation to $e = 0$ occurs slightly later than for $\epsilon = 0$. The switching plane can be described by

$$\varphi = x_I(e + x_I \epsilon) = 0 \tag{4}$$

and is graphically shown in Fig. 6 for $\epsilon = 0$ and $\epsilon > 0$. This adapted switching results in the output of the SPANI according to

$$u_s = \begin{cases} x_I, & \text{if } \varphi > 0 \\ -x_I, & \text{if } \varphi < 0 \end{cases} \tag{5}$$

Authorized licensed use limited to: Eindhoven University of Technology. Downloaded on May 02,2021 at 14:18:11 UTC from IEEE Xplore. Restrictions apply.

This article has been accepted for inclusion in a future issue of this journal. Content is final as presented, with the exception of pagination.

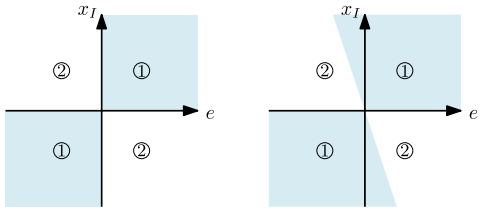

(a) $\varphi = ex_I$ (b) $\varphi = x_I(x_I\epsilon + e)$

Fig. 6. (e, x_I)-plane for tilting parameter $\epsilon = 0$ (left) and $\epsilon > 0$ (right). In mode 1, $\varphi > 0$; in mode 2, $\varphi < 0$. (a) $\varphi = ex_I$. (b) $\varphi = x_I(x_I\epsilon + e)$.

which are referred to as modes 1 and 2, respectively, in Fig. 6. The design choice for $\epsilon > 0$ is based on the fact that at the desired state of the system, it holds that $e = 0$. For $\epsilon = 0$, this means that the desired state is on the switching plane, resulting in a switching integrator action for every perturbation from the desired state.

Remark 2: As indicated above, the rationale behind including a tilting factor $\epsilon > 0$ in the definition of the switching plane is to prevent switching as a result of small perturbations around desired equilibrium points $(e^\star, x_I^\star)$, where $e^\star = 0$. Nonetheless, the pair $(e, x_I) = (0, 0)$ still lies on the switching plane even if $\epsilon > 0$. It should, however, be noted that $e^\star = 0$ is typically achieved, for example, in the presence of constant disturbances, by means of integral action, and thus, $x_I^\star \neq 0$. As a result, the pair $(e, x_I) = (0, 0)$ is typically not a desired equilibrium of the system.

For a more detailed explanation of the rationale behind introducing this ϵ parameter, please refer to [16]. A drawback associated with the use of this tilting parameter $\epsilon > 0$ is the potentially decreased transient performance compared to the case where $\epsilon = 0$. This is because when $\epsilon > 0$, the switch in u_s occurs later than the case where $\epsilon = 0$, and thus, the buffer of the integrator results in larger overshoot.

3) F-SPANI: Let us now introduce the F-SPANI, which uses the phase branch of the SPAN to anticipate an error sign switch. In terms of the SPAN filter, the F-SPANI uses

$$\mathcal{H}_1 = \mathcal{C}_I \quad \mathcal{H}_2 = \mathcal{C}_f \tag{6}$$

with $\mathcal{C}_f$ a filter that provides phase lead. The switching parameter ϵ is still used, since for $e = 0$, we have $u_f = 0$ as well, where u_f is the output of $\mathcal{C}_f$ (see Fig. 7). The motivation for the F-SPANI is to use the phase branch to further improve the transient performance compared to the SPANI. The main performance limitation of a linear integrator is the phase lag of 90°. By now adding phase lead in the phase branch and using only the amplitude of the integrator in the magnitude branch, the advantages of the integrator can be used in terms of steady-state tracking performance, without suffering from a large phase lag that results in overshoot. Insights of this beneficial property of the F-SPANI will be provided in Section III-C by means of a describing function analysis.

Compared with the SPANI, in the F-SPANI, the switching law has changed from a dependence on the error signal e to a dependence on the output u_f of the filter with phase

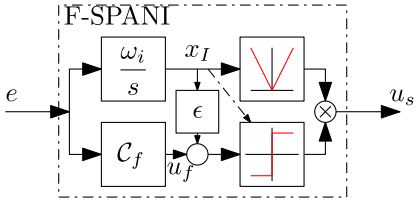

Fig. 7. F-SPANI filter.

lead. This results in causal anticipation of the changing sign of the error and therefore potentially in further reduction of the overshoot compared to the SPANI. By switching the sign of the integrator buffer before the switch in the error sign occurs, the integrator can start counteracting the overshoot in advance, hence reducing the overshoot.

III. Analysis of Closed-Loop Properties

In Section II, an overview of the design and the working principle of the hybrid controller F-SPANI were given. In this section, we will study the closed-loop properties induced by this control strategy. In Section III-A, the closed-loop system is described in state-space form. In Section III-B, the conditions for closed-loop stability will be presented. In Section III-C, a describing function analysis is provided, which gives additional insights into the working principle of this novel hybrid controller. In Section III-D, we conclude with a numerical example, illustrating the full potential of the method.

A. Closed-Loop System Description

In a closed-loop feedback configuration, the SPANI and the F-SPANI can be introduced as in Fig. 8. Note that the SPANI is a special case of the F-SPANI when $\mathcal{C}_f = 1$.

The feedback controller in Fig. 8 is slightly adjusted compared to the results in [16] and [17]. A low-pass filter ($\mathcal{L}$) and a notch filter ($\mathcal{N}$) have been included explicitly, separated from the nominal controller ($\mathcal{C}_{\text{nom}}$). The motivation for this change can be found in [17], where it has been shown that resonance peaks in the plant dynamics $\mathcal{P}$ can cause significant limitations on the achievable performance, which can be avoided with the use of a notch filter. For the situation where the notch filter and the low-pass filter are included in $\mathcal{C}_{\text{nom}}$, resonant peaks, high-frequency oscillations, and measurement noise are only suppressed in the path of the nominal controller. As a result, these undesired effects are then passed through the F-SPANI in an unfiltered fashion, which will result in undesired switches and reduced performance. With the design choice to place the notch and low-pass filters in the closed-loop control structure before the parallel structure with the F-SPANI element, these effects are filtered in both branches of the loop.

In terms of mathematical modeling, the closed-loop configuration in Fig. 8 can be defined by the state-space models of each of the components. In each of these models, x represents the state of the component, A represents the system matrix, B represents the input matrix, C represents the output matrix, and D represents the direct feedthrough matrix, all real matrices

Authorized licensed use limited to: Eindhoven University of Technology. Downloaded on May 02,2021 at 14:18:11 UTC from IEEE Xplore. Restrictions apply.

This article has been accepted for inclusion in a future issue of this journal. Content is final as presented, with the exception of pagination.

with the appropriate subscripts and dimensions, depending on the considered component. The signals u represent the internal input signals, which are the outputs of each of the controller components, as shown in Fig. 8. The plant is defined by

$$\mathcal{P}: \begin{cases} \dot{x}_p = A_p x_p + B_p(d+u) \\ y_p = C_p x_p \end{cases} \tag{7}$$

where the subscript p indicates that it is related to the plant, $x_p \in \mathbb{R}^{n_{x_p}}$ is the plant state, $d \in \mathbb{R}^{n_d}$ is the (external) disturbance, $u = u_s + u_c$ is the controller output taking values in $\mathbb{R}^{n_u}$, and $y_p \in \mathbb{R}^{n_{y_p}}$ is the plant output. Similarly, the nominal linear controller, indicated by subscript c, is defined by

$$\mathcal{C}_{\text{nom}}: \begin{cases} \dot{x}_c = A_c x_c + B_c u_l \\ u_c = C_c x_c + D_c u_l \end{cases} \tag{8}$$

where $x_c \in \mathbb{R}^{n_{x_c}}$ is the controller state and $u_l \in \mathbb{R}^{n_{u_l}}$ is the notch- and low-pass filtered error signal. The low-pass filter, indicated by the subscript l, is given by

$$\mathcal{L}: \begin{cases} \dot{x}_l = A_l x_l + B_l u_n \\ u_l = C_l x_l + D_l u_n \end{cases} \tag{9}$$

where $x_l \in \mathbb{R}^{n_{x_l}}$ is the low-pass filter state and $u_n \in \mathbb{R}^{n_{u_n}}$ is the output of the notch filter. The notch filter, which may contain multiple resonances and antiresonances, is defined by

$$\mathcal{N}: \begin{cases} \dot{x}_n = A_n x_n + B_n e \\ u_n = C_n x_n + D_n e \end{cases} \tag{10}$$

where $x_n \in \mathbb{R}^{n_{x_n}}$ is the notch filter's state and $e = r - y_p$ is the closed-loop tracking error, with $r \in \mathbb{R}^{n_{y_p}}$ the reference signal.

The F-SPANI as shown in Fig. 8 is defined by

$$\text{F-SPANI:} \begin{cases} \dot{x}_I = \omega_i u_l \\ u_s = \begin{cases} x_I, & \text{if } x_I(\epsilon x_I + u_f) > 0 \\ -x_I, & \text{if } x_I(\epsilon x_I + u_f) < 0 \end{cases} \end{cases} \tag{11}$$

where $x_I \in \mathbb{R}$ is the F-SPANI's state and $u_f \in \mathbb{R}$ is the output of the filter $\mathcal{C}_f$ designed for phase lead and defined by

$$\mathcal{C}_f: \begin{cases} \dot{x}_f = A_f x_f + B_f u_l \\ u_f = C_f x_f + D_f u_l \end{cases} \tag{12}$$

with $x_f \in \mathbb{R}^{n_{x_f}}$. This filter can be any filter that results in a phase lead, e.g., a (or multiple) lead filter(s).

Using the individual system components described above, the closed-loop system in Fig. 8 can be described as follows:

$$\dot{x} = \begin{cases} A_1 x + B_r r + B_d d, & \text{if } x_I(\epsilon x_I + u_f) > 0 \quad (13a) \\ A_2 x + B_r r + B_d d, & \text{if } x_I(\epsilon x_I + u_f) < 0 \quad (13b) \end{cases}$$

with inputs r and d, $x = \begin{bmatrix} x_p^\top & x_c^\top & x_l^\top & x_n^\top & x_I^\top & x_f^\top \end{bmatrix}^\top \in \mathbb{R}^n$, and where the system matrices in (13) are given by (14) and (15), as shown at the bottom of the page, and input matrices

$$B_r = \begin{bmatrix} B_p D_c D_l D_n \\ B_c D_l D_n \\ B_l D_n \\ B_n \\ \omega_i D_l D_n \\ B_f D_l D_n \end{bmatrix}, \quad B_d = \begin{bmatrix} B_p \\ 0 \\ 0 \\ 0 \\ 0 \\ 0 \end{bmatrix}. \tag{16}$$

The system matrix A_1 defines the dynamics in the first mode in Fig. 6 and A_2 the second mode. Note that the matrices A_1 and A_2 are almost identical with their only difference being the sign difference in their $(1,5)$ block. The output of the closed-loop system is given by

$$y_p = C_p x_p = \begin{bmatrix} I & 0 & 0 & 0 & 0 & 0 \end{bmatrix} x. \tag{17}$$

Note that when the dynamics according to A_1 are active, the system's dynamics are assumed to be asymptotically stable by design, i.e., A_1 is Hurwitz (all eigenvalues in the open left half-plane). In particular, these dynamics can be tuned by the controller components ($\mathcal{C}_{\text{nom}}$, $\mathcal{N}$, $\mathcal{L}$, $\mathcal{C}_f$, and ω_i) designed by the user. A thorough analysis of the stability of the hybrid closed-loop dynamics is given in Section III-B.

Solutions to (13) will be considered in Filippov sense (see [18]). To do so, we extend (13) to the differential inclusion

$$\dot{x} \in \begin{cases} \{A_1 x + B_r r + B_d d\}, & \text{if } \psi > 0 \\ \text{co}(A_1 x, A_2 x) + B_r r + B_d d, & \text{if } \psi = 0 \\ \{A_2 x + B_r r + B_d d\}, & \text{if } \psi < 0 \end{cases} \tag{18}$$

where $\psi = x_I(\epsilon x_I + u_f)$ and $\text{co}(A_1 x, A_2 x)$ denotes the convex hull $\{\lambda A_1 x + (1-\lambda) A_2 x,\ \lambda \in [0,1]\}$. The formulation in (18) allows for the convex combination of vector fields in (13) to be active on the switching plane (where $\psi = 0$), thereby allowing possible sliding modes (see [18] for details). Solutions to the closed-loop system are now defined as locally absolutely continuous functions, satisfying (18) almost everywhere. This

$$A_1 = \begin{bmatrix} A_p - B_p D_c D_l D_n C_p & B_p C_c & B_p D_c C_l & B_p D_c D_l C_n & B_p & 0 \\ -B_c D_l D_n C_p & A_c & B_c C_l & B_c D_l C_n & 0 & 0 \\ -B_l D_n C_p & 0 & A_l & B_l C_n & 0 & 0 \\ -B_n C_p & 0 & 0 & A_n & 0 & 0 \\ -\omega_i D_l D_n C_p & 0 & \omega_i C_l & \omega_i D_l C_n & 0 & 0 \\ -B_f D_l D_n C_p & 0 & B_f C_l & B_f D_l C_n & 0 & A_f \end{bmatrix} \tag{14}$$

$$A_2 = \begin{bmatrix} A_p - B_p D_c D_l D_n C_p & B_p C_c & B_p D_c C_l & B_p D_c D_l C_n & -B_p & 0 \\ -B_c D_l D_n C_p & A_c & B_c C_l & B_c D_l C_n & 0 & 0 \\ -B_l D_n C_p & 0 & A_l & B_l C_n & 0 & 0 \\ -B_n C_p & 0 & 0 & A_n & 0 & 0 \\ -\omega_i D_l D_n C_p & 0 & \omega_i C_l & \omega_i D_l C_n & 0 & 0 \\ -B_f D_l D_n C_p & 0 & B_f C_l & B_f D_l C_n & 0 & A_f \end{bmatrix} \tag{15}$$

Authorized licensed use limited to: Eindhoven University of Technology. Downloaded on May 02,2021 at 14:18:11 UTC from IEEE Xplore. Restrictions apply.

This article has been accepted for inclusion in a future issue of this journal. Content is final as presented, with the exception of pagination.

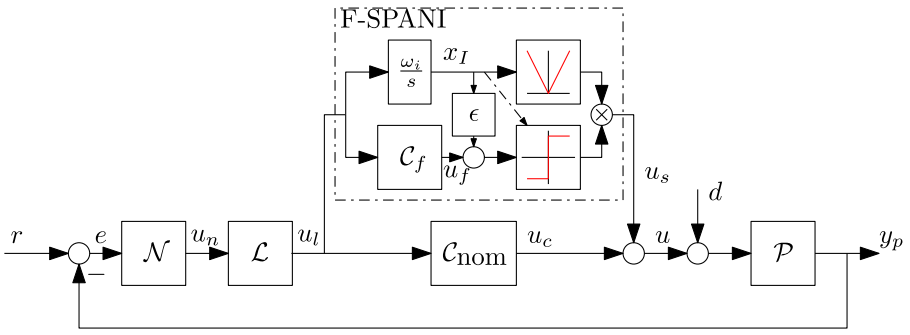

Fig. 8. F-SPANI filter in a typical control configuration.

indeed corresponds to the notion of Filippov solutions [18] (for more detailed discussions on generalized solutions to hybrid dynamical systems and differential inclusions, see [18]–[21]).

B. Stability Analysis

In this section, we present a stability result for the F-SPANI, which is also applicable to the special case of the SPANI. A coordinate transformation is proposed, i.e.

$$\tilde{x} = x - x^*, \tag{19}$$

where x^* represents the equilibrium of the system, which is defined by

$$\dot{x}|_{x=x^*} = A_1 x^* + B_r r_s + B_d d_s = 0 \tag{20}$$

for a constant reference $r_s \in \mathbb{R}$ and a constant disturbance $d_s \in \mathbb{R}$.

Definition 1: For a fixed disturbance $d_s \in \mathbb{R}$ and a fixed reference $r_s \in \mathbb{R}$, the equilibrium x^* of (18) is said to be globally exponentially stable (GES) if there exist $c \in \mathbb{R}_{>0}$ and $\mu \in \mathbb{R}_{>0}$ such that all Filippov solutions $x : \mathbb{R}_{\geq 0} \mapsto \mathbb{R}^n$ to (18) satisfy $\|x(t) - x^*\| \leq ce^{-\mu t}\|x(0) - x^*\|$, for all $t \in \mathbb{R}_{\geq 0}$.

The conditions presented in Theorem 1 will turn out to be sufficient for verifying GES of the equilibrium x^* of the closed-loop system. Before stating the main theorem of this section, let us first introduce a few definitions. Given a symmetric positive definite matrix $P \in \mathbb{R}^{n\times n}$ (which will be used for building a common quadratic Lyapunov function (CQLF) [22]), the matrix Q is defined by

$$Q = \begin{bmatrix} A_2^\top P + PA_2 & PA_dA_1^{-1}B_r & PA_dA_1^{-1}B_d \\ \star & 0 & 0 \\ \star & \star & 0 \end{bmatrix} \tag{21}$$

where $\star$ is used to define the symmetry in the matrix, i.e., $\begin{bmatrix} a & b \\ b^\top & c \end{bmatrix} = \begin{bmatrix} a & b \\ \star & c \end{bmatrix}$, and where $A_d = A_1 - A_2$. Furthermore, a matrix R is given by (22), as shown at the bottom of the page, with $\alpha := \epsilon\gamma_r + C_f\xi_r + D_fC_l\delta_r + D_fD_lC_n\eta_r$ and $\beta := \epsilon\gamma_d + C_f\xi_d + D_fC_l\delta_d + D_fD_lC_n\eta_d$. The variables γ_r, γ_d, ξ_r, ξ_d, δ_r, δ_d, η_r, and η_d define the following equilibrium states:

$$\begin{aligned} x_I^* &= \gamma_r r_s + \gamma_d d_s, \quad x_f^* = \xi_r r_s + \xi_d d_s \\ x_l^* &= \delta_r r_s + \delta_d d_s, \quad x_n^* = \eta_r r_s + \eta_d d_s \end{aligned} \tag{23}$$

which implies that

$$\begin{aligned} \delta_r &= [0_{1\times n_{x_p}} 0_{1\times n_{x_c}} - I_{1\times n_{x_l}} 0_{1\times n_{x_n}} 0_{1\times 1}\ 0_{1\times n_{x_f}}]A_1^{-1}B_r \\ \eta_r &= [0_{1\times n_{x_p}} 0_{1\times n_{x_c}} 0_{1\times n_{x_l}} - I_{1\times n_{x_n}} 0_{1\times 1}\ 0_{1\times n_{x_f}}]A_1^{-1}B_r \\ \gamma_r &= [0_{1\times n_{x_p}} 0_{1\times n_{x_c}} 0_{1\times n_{x_l}} 0_{1\times n_{x_n}} - I_{1\times 1}\ 0_{1\times n_{x_f}}]A_1^{-1}B_r \\ \xi_r &= [0_{1\times n_{x_p}} 0_{1\times n_{x_c}} 0_{1\times n_{x_l}} 0_{1\times n_{x_n}} 0_{1\times 1}\ - I_{1\times n_{x_f}}]A_1^{-1}B_r. \end{aligned} \tag{24}$$

The variables δ_d, η_d, γ_d, and ξ_d can be computed in a similar manner as in (24) but are postmultiplied by B_d instead of B_r. Note that since A_1 is assumed to be Hurwitz by design,

$$R = \begin{bmatrix} 0_{n_{x_p}\times n_{x_p}} & 0_{n_{x_p}\times n_{x_c}} & 0_{n_{x_p}\times n_{x_l}} & 0_{n_{x_p}\times n_{x_n}} & -\frac{1}{2}C_p^\top D_n^\top D_l^\top D_f^\top & 0_{n_{x_p}\times n_{x_f}} & -\frac{1}{2}C_p^\top D_n^\top D_l^\top D_f^\top\gamma_r & -\frac{1}{2}C_p^\top D_n^\top D_l^\top D_f^\top\gamma_d \\ \star & 0_{n_{x_c}\times n_{x_c}} & 0_{n_{x_c}\times n_{x_l}} & 0_{n_{x_c}\times n_{x_n}} & 0_{n_{x_c}\times 1} & 0_{n_{x_c}\times n_{x_f}} & 0_{n_{x_c}\times 1} & 0_{n_{x_c}\times 1} \\ \star & \star & 0_{n_{x_l}\times n_{x_l}} & 0_{n_{x_l}\times n_{x_n}} & \frac{1}{2}C_l^\top D_f^\top & 0_{n_{x_l}\times n_{x_f}} & \frac{1}{2}C_l^\top D_f^\top\gamma_r & \frac{1}{2}C_l^\top D_f^\top\gamma_d \\ \star & \star & \star & 0_{n_{x_n}\times n_{x_n}} & \frac{1}{2}C_n^\top D_l^\top D_f^\top & 0_{n_{x_n}\times n_{x_f}} & \frac{1}{2}C_n^\top D_l^\top D_f^\top\gamma_r & \frac{1}{2}C_n^\top D_l^\top D_f^\top\gamma_d \\ \star & \star & \star & \star & \epsilon & \frac{1}{2}C_f & \frac{1}{2}\epsilon\gamma_r + \frac{1}{2}\alpha & \frac{1}{2}\epsilon\gamma_d + \frac{1}{2}\beta \\ \star & \star & \star & \star & \star & 0_{n_{x_f}\times n_{x_f}} & \frac{1}{2}C_f^\top\gamma_r & \frac{1}{2}C_f^\top\gamma_d \\ \star & \star & \star & \star & \star & \star & \gamma_r\alpha & \frac{1}{2}\gamma_r\beta + \frac{1}{2}\gamma_d\alpha^\top \\ \star & \star & \star & \star & \star & \star & \star & \gamma_d\beta \end{bmatrix} \tag{22}$$

Authorized licensed use limited to: Eindhoven University of Technology. Downloaded on May 02,2021 at 14:18:11 UTC from IEEE Xplore. Restrictions apply.

This article has been accepted for inclusion in a future issue of this journal. Content is final as presented, with the exception of pagination.

it is invertible, and thus, the equlibrium solution $x^\star$ to (20) is unique. Finally, let the matrix M be given by

$$M = \begin{bmatrix} I_{n\times n} & 0_{n\times 1} \\ 0_{2\times n} & \begin{bmatrix}\gamma_r \\ \gamma_d\end{bmatrix} \end{bmatrix}, \quad \text{with } \begin{bmatrix}\gamma_r \\ \gamma_d\end{bmatrix} \neq 0_{2\times 1}. \tag{25}$$

Theorem 1: Consider the differential inclusion (18) for some positive tilting factor $\epsilon > 0$ and a Hurwitz matrix A_1. Let $r_s \in \mathbb{R}$ be a constant reference signal and $d_s \in \mathbb{R}$ be a constant disturbance signal. If there exist a positive definite matrix $P = P^\top \succ 0$ and a constant $\theta \geq 0$ satisfying

$$A_1^\top P + P A_1 \prec 0 \tag{26}$$

$$M^\top (Q - \theta R) M \prec 0, \tag{27}$$

then the equilibrium point x^* given by (20) for the system (18), satisfying $e^* = r_s - C_p x_p^* = 0$, is GES in the sense of Definition 1.

Proof: The proof of Theorem 1 is based on the use of the CQLF (see [22]–[27] for detailed discussions on the application of common Lyapunov functions to the stability analysis of switched and piecewise smooth systems)

$$V(\tilde{x}) = \tilde{x}^\top P \tilde{x}. \tag{28}$$

In particular, in order to prove GES of the system, first, let us make the observation that

$$\lambda_{\min}(P)\|\tilde{x}(t)\|^2 \leq V(\tilde{x}(t)) \leq \lambda_{\max}(P)\|\tilde{x}(t)\|^2 \tag{29}$$

where $\lambda_{\min}(P)$ and $\lambda_{\max}(P)$ denote the minimum and maximum eigenvalue of P, respectively. Moreover, we will prove that the time derivative of the Lyapunov function $t \mapsto V(\tilde{x}(t))$ along Filippov solutions to (18) satisfies almost everywhere

$$\dot{V}(\tilde{x}) \leq -c\|\tilde{x}\|^2 \tag{30}$$

(where we have omitted time dependence for convenience of notation) for some $c > 0$ (irrespective of the mode of operation). The proof consists of three cases.

1) Mode 1 is active, i.e., $\dot{x} = A_1 x + B_r r + B_d d$, and hence, $x_I(\epsilon x_I + u_f) > 0$.
2) Mode 2 is active, i.e., $\dot{x} = A_2 x + B_r r + B_d d$, and hence, $x_I(\epsilon x_I + u_f) < 0$.
3) The system is at the switching plane, i.e., $x_I(\epsilon x_I + u_f) = 0$ and $\dot{x} = \lambda A_1 x + (1-\lambda)A_2 x + B_r r + B_d d$ for some $\lambda \in [0, 1]$.

1) Case 1 ($x_I(\epsilon x_I + u_f) > 0$): In the transformed coordinates in (19), the dynamics of the system are given by

$$\dot{\tilde{x}} = A_1 \tilde{x} \tag{31}$$

where we have used (20). The time derivative of the Lyapunov function V, along solutions of (31), satisfies, due to (26)

$$\dot{V}(\tilde{x}) = \tilde{x}^\top \left(A_1^\top P + P A_1\right)\tilde{x} \leq -c_+\|\tilde{x}\|^2 \tag{32}$$

for some $c_+ > 0$.

2) Case 2 ($x_I(\epsilon x_I + u_f) < 0$): . In the transformed coordinates, the dynamics of the system are given by

$$\dot{\tilde{x}} = \underbrace{A_2 x + B_r r_s + B_d d_s}_{\dot{x} \text{ in (13b)}} \underbrace{- A_1 x^* - B_r r_s - B_d d_s}_{=0 \text{ due to (20)}} \tag{33}$$

$$= A_2 x - A_1 x^* \tag{34}$$

$$= A_2 \tilde{x} - (A_1 - A_2)x^* =: A_2 \tilde{x} - A_d x^*. \tag{35}$$

The time derivative of (28) along the solutions of (35) is now given by

$$\dot{V}(\tilde{x}) = \tilde{x}^\top A_2^\top P \tilde{x} - x^{*\top} A_d^\top P \tilde{x} + \tilde{x}^\top P A_2 \tilde{x} - \tilde{x}^\top P A_d x^*. \tag{36}$$

This time derivative of the Lyapunov function can be expressed in terms of the transformed states $\tilde{x}$ and the external inputs of the system r_s and d_s. Using (20), it is deduced that

$$x^* = -A_1^{-1}(B_r r_s + B_d d_s) \tag{37}$$

where we use that A_1 is Hurwitz and thus nonsingular. By using (37) and reworking (36), we find

$$\dot{V}(\tilde{x}) = \tilde{x}_a^\top Q \tilde{x}_a \tag{38}$$

where $\tilde{x}_a$ is the augmented state vector defined by $\tilde{x}_a = \left[\tilde{x}^\top \; r_s^\top \; d_s^\top\right]^\top$ and Q as defined in (21).

In support of the stability analysis, we now aim to show that the right-hand side of (38) satisfies for some $c_- > 0$

$$\tilde{x}_a^\top Q \tilde{x}_a \leq -c_-\|\tilde{x}\|^2 \tag{39}$$

for all $\tilde{x}_a$ when $\psi = x_I(\epsilon x_I + u_f) \leq 0$ (note that for case 2, it suffices to show (39) for $\psi < 0$; however, since the results below are also useful in showing (30) for case 3, we consider $\psi \leq 0$). Similar to the time derivative of the Lyapunov function, also the switching rule can be given by a quadratic relation of the augmented states $\tilde{x}_a$. In particular, by using (23), the switching function $\psi = x_I(\epsilon x_I + u_f)$ can be written in the quadratic form

$$\psi = \tilde{x}_a^\top R \tilde{x}_a \tag{40}$$

with R as in (22). Using the above formulations, we now aim to establish

$$\tilde{x}_a^\top Q \tilde{x}_a \leq -c_-\|\tilde{x}\|^2 \quad \text{when } \tilde{x}_a^\top R \tilde{x}_a \leq 0 \tag{41}$$

for some $c_- > 0$. To prove this, consider the matrices M as in (25) and

$$G = \begin{bmatrix} 0_{n\times 1} \\ -\gamma_d \\ \gamma_r \end{bmatrix}. \tag{42}$$

Using these matrices, the augmented state vector can be written as

$$\tilde{x}_a = \begin{bmatrix} \tilde{x} \\ r_s \\ d_s \end{bmatrix} = M\tilde{m} + g \tag{43}$$

for some $\tilde{m} \in \mathbb{R}^{(n+1)\times 1}$ and $g \in \text{im}(G)$ and where it can be shown using basic algebra that $\text{im}(G) \subseteq \ker(Q)$, with Q as in (21), where for a general matrix $\mathcal{G} \in \mathbb{R}^{n_g \times m_g}$, we use $\text{im}(\mathcal{G}) := \{\mathcal{G}a \mid a \in \mathbb{R}^{m_g}\}$ and $\ker(\mathcal{G}) := \{a \in \mathbb{R}^{m_g} \mid$

Authorized licensed use limited to: Eindhoven University of Technology. Downloaded on May 02,2021 at 14:18:11 UTC from IEEE Xplore. Restrictions apply.

This article has been accepted for inclusion in a future issue of this journal. Content is final as presented, with the exception of pagination.

$\mathcal{G}a = 0\}$. Using these properties, the time derivative $\dot{V}(\tilde{x})$ in (38) satisfies

$$\begin{aligned}\tilde{x}_a^\top Q\tilde{x}_a &= (\tilde{m}^\top M^\top + g^\top)Q(M\tilde{m} + g)\\ &= \tilde{m}^\top M^\top QM\tilde{m} + \underbrace{\tilde{m}^\top M^\top Qg}_{=0} + \underbrace{g^\top QM\tilde{m}}_{=0} + \underbrace{g^\top Qg}_{=0}\end{aligned} \tag{44}$$

and thus, $\dot{V}(\tilde{x})$ satisfies (41) if and only if

$$\tilde{x}_a^\top Q\tilde{x}_a = \tilde{m}^\top M^\top QM\tilde{m} \leq -c_-\|\tilde{x}\|^2 \quad \text{when } \tilde{x}_a^\top R\tilde{x}_a \leq 0. \tag{45}$$

Similarly, it can be shown that $\mathrm{im}(G) \subseteq \ker(R)$, with R as in (22), using (45) results in the requirement

$$\tilde{m}^\top M^\top QM\tilde{m} \leq -c_-\|\tilde{x}\|^2 \quad \text{when } \tilde{m}^\top M^\top RM\tilde{m} \leq 0 \tag{46}$$

which is guaranteed when

$$\tilde{m}^\top M^\top (Q - \theta R)M\tilde{m} \leq -c_m\|\tilde{m}\|^2 \tag{47}$$

for some $\theta \geq 0$ and $c_m > 0$. As (47) follows from (27) and $\theta \geq 0$, we also have (30) for case 2.

3) Case 3 ($x_I(\epsilon x_I + u_f) = 0$): In this case, it holds almost everywhere that

$$\dot{V}(\tilde{x}) = \lambda\tilde{x}^\top\big(A_1^\top P + PA_1\big)\tilde{x} + (1-\lambda)\tilde{x}_a^\top Q\tilde{x}_a \tag{48}$$

for some $\lambda \in [0, 1]$. It can be observed from case 1 that

$$\lambda\tilde{x}^\top\big(A_1^\top P + PA_1\big)\tilde{x} \leq -\lambda c_+\|\tilde{x}\|^2 \tag{49}$$

which is satisfied as a result of (32), and

$$(1-\lambda)\tilde{x}_a^\top Q\tilde{x}_a \leq -(1-\lambda)c_-\|\tilde{x}\|^2 \tag{50}$$

from (41) and (45) as $\tilde{x}_a^\top R\tilde{x}_a = 0$. Hence, it can be concluded that (48) is bounded almost everywhere by

$$\dot{V}(\tilde{x}) \leq -c\|\tilde{x}\|^2, \quad \text{with } c = \min(c_-, c_+). \tag{51}$$

Based on the analysis performed above, we observe that (30) holds with $c = \min(c_-, c_+)$ and a CQLF $V(\tilde{x}) = \tilde{x}^\top P\tilde{x}$ (irrespective of the mode of operation). Through straightforward algebraic manipulations of (29) and (30), it follows that:

$$\|\tilde{x}(t)\| \leq \sqrt{\frac{\lambda_{\max}(P)}{\lambda_{\min}(P)}}e^{\frac{-c}{2\lambda_{\max}(P)}t}\|\tilde{x}(0)\| \tag{52}$$

along all Filippov solutions of the differential inclusion (18), indicating that the equilibrium x^* is GES. □

Remark 3: Note that the matrix R is a function of the tilting parameter ϵ, and therefore, an iterative process can be used to find the "best" value for ϵ while guaranteeing that the system is GES. In this work, a bisection algorithm has been used [28]. The "best" value for ϵ, in this case, is defined as the smallest value for which the LMIs are feasible. The value of ϵ defines the delay of the switch, compared to switching when $e = 0$, which should be as small as possible. Moreover, note that, since the feasibility of the inequalities (26) and (27) implies the existence of a CQLF, the value found for ϵ via the method described above can be conservative, that is, the smallest value for ϵ such that (18) is GES can be lower than the one found using the bisection algorithm.[1] As such, in applications where one is aiming for maximizing the performance of the F-SPANI controller, one can try to further reduce ϵ, using the value returned by the bisection algorithm as a starting point. It should, however, be noted that in such scenarios, stability is not guaranteed by Theorem 1 and care should be taken (e.g., via extensive simulations/experiments representative of real-life operational conditions). Moreover, lowering ϵ is likely to result in reduction of robustness of the system with respect to perturbations. As such, when tuning the value of ϵ, there exists a tradeoff between transient performance and robustness that should be addressed given the particular problem at hand. In any case, it is not recommended to reduce ϵ down to $\epsilon = 0$, as doing so would completely eliminate robustness properties, leading to unwanted switching as a result of small perturbations around the desired equilibrium points.

C. Describing Function Analysis

In this section, a describing function analysis [29] of the hybrid controllers introduced in Section II is given. This describing function analysis provides further insight into the benefits of the controllers in the frequency domain.

To obtain the describing function of a nonlinear filter numerically, a harmonic signal is applied to the filter with varying frequencies. The amplitude of the harmonic signal remains constant for all frequencies since the F-SPANI only influences the phase of the signal, not the amplitude, compared to the linear integrator. The output of the filter is evaluated, and the first harmonic of the output response, i.e., the frequency corresponding to the injected harmonic input, is analyzed in terms of its amplitude and phase (with respect to the harmonic input). Note that only the integrator parts of the closed loop are considered, i.e., the parts shown in Figs. 5 and 7 for the SPANI and the F-SPANI, respectively, compared to the response of a linear integrator defined by $\mathcal{C}_I \overset{(6)}{=} (\omega_i/s)$.

In Fig. 9, a time-domain visualization of the interpretation of the describing function is shown for the F-SPANI at 1 Hz. The blue line indicates the input to the F-SPANI, which results in the output indicated by the red line. The first harmonic of this signal corresponds to the yellow line. It can be seen that the yellow line does not describe the response accurately; however, it gives some "linear interpretation" of the nonlinear control element. The F-SPANI is tuned according to

$$\omega_i = 5 \text{ [rad/s]} \quad \epsilon = 0.2 \quad \mathcal{C}_f(s) = \frac{s + 60\pi}{s + 3.3333\pi}. \tag{53}$$

The SPANI uses the same parameters as in (53), however, with $\mathcal{C}_f = 1$.

In Fig. 10, the approximated response, numerically obtained with the describing function approach, for a wide frequency band is shown in the frequency domain using only the F-SPANI, i.e., from u_l to u_s in Fig. 8 or from e to u_s in Fig. 7. Let us note that since we simulate the F-SPANI in open loop, no sliding modes occur in this setting. It can be seen that a

[1] An interesting future research direction is to extend the stability result in Theorem 1 such that tighter bounds on ϵ are found by considering more flexible Lyapunov functions, e.g., piecewise quadratic Lyapunov functions.

Authorized licensed use limited to: Eindhoven University of Technology. Downloaded on May 02,2021 at 14:18:11 UTC from IEEE Xplore. Restrictions apply.

This article has been accepted for inclusion in a future issue of this journal. Content is final as presented, with the exception of pagination.

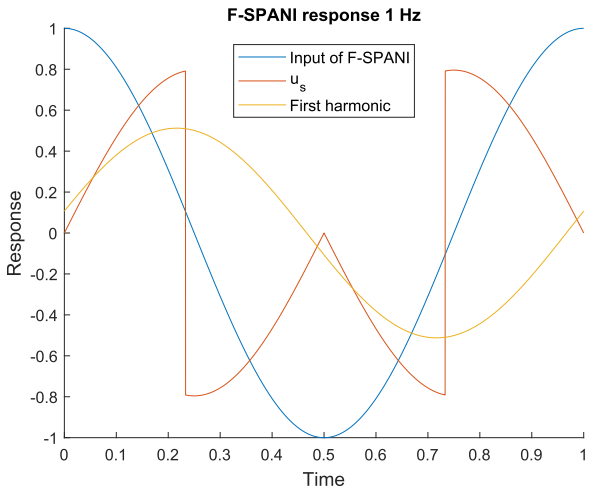

Fig. 9. Time-domain outputs for 1 Hz.

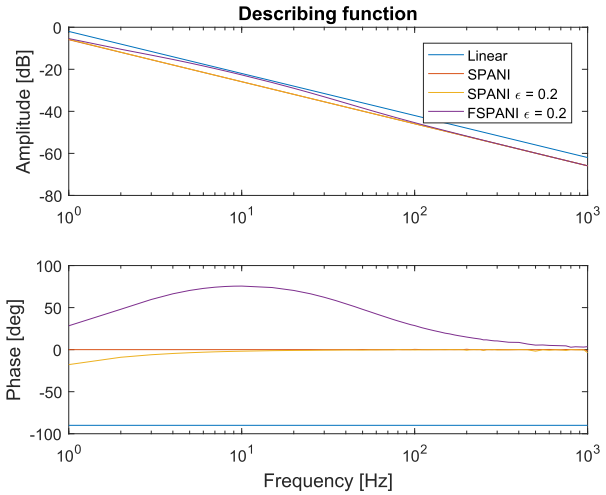

Fig. 10. Describing function without low-pass and notch filter.

linear filter, as expected, shows a slope of -1, i.e., -20 dB per decade, and a phase of $-90°$ for all frequencies. The SPANI with $\epsilon = 0$, which is included for completeness (but should not be applied in practice due to unwanted oscillations), also shows a -1 slope, at a slightly lower amplitude, however, with a phase of 0° over all frequencies. This effect can be attributed to the fact that the switch is made exactly at the point where the harmonic input switches sign. The addition of the ϵ parameter in the SPANI results in a slight phase drop, mainly for lower frequencies. The F-SPANI shows a clear effect of the lead filter. The lead filter was designed around 10 Hz with a maximal phase lead of 53°. At 10 Hz, it can be observed that the F-SPANI has a significant phase lead, and also, the amplitude of the first harmonic of the F-SPANI is almost identical to the linear response.

By analyzing these results, it is concluded that the F-SPANI is indeed expected to provide the largest improvement in transient performance from all of these filters.

Remark 4: It can be seen that the first harmonic, as shown in Fig. 9, does not describe the response u_s of the filter accurately; however, it is the main component in the frequency domain, which gives valuable (though approximate) insights of what the filter does in the linear sense. It should be noted that the describing function of the F-SPANI is only used for gaining such insights and does not play a role in the stability analysis of the closed-loop system. Using more advanced identification techniques, a best linear approximation could be obtained, where all frequencies are excited at the same time, which can also result in an approximation of the influence of the nonlinearities on the linear approximation [30].

D. Numerical Example

In this section, we show the potential of the F-SPANI compared to the linear controller and the SPANI on a numerical example consisting of a second-order plant with the transfer function

$$P(s) = \frac{355.30}{s^2 + 2.639s + 355.3}. \tag{54}$$

Using this model, a simulation has been performed using a linear controller, the SPANI controller from Section II-B2, and the F-SPANI controller from Section II-B3. The controllers, as shown in Fig. 8, are designed as

$$\mathcal{N}(s) = 1 \qquad \mathcal{L}(s) = \frac{1}{0.001989s + 1} \tag{55}$$

$$\mathcal{C}_{\text{nom}}(s) = \frac{29.02s + 1148}{s + 188.5} \quad \mathcal{C}_f(s) = \frac{0.04775s + 1}{0.005305s + 1} \tag{56}$$

$$\omega_i = 67.5442. \tag{57}$$

The parameter ϵ has been selected for both the SPANI and F-SPANI individually using a bisection algorithm, as discussed in Remark 3. The obtained value for ϵ is the lowest value that guarantees global exponential stability using the results obtained in Theorem 1. For this simulation study, the values for ϵ obtained by the bisection algorithm were 0.2285 and 0.2854 for the SPANI and the F-SPANI, respectively. However, as discussed in Remark 3, since Theorem 1 provides stability guarantees based on the construction of a common Lyapunov function, the values found for ϵ can be conservative. Thus, some fine-tuning is possible to further lower ϵ (without losing stability based on simulations), resulting in slightly better transient performance without introducing undesired switches, as is the case for $\epsilon = 0$.

In Fig. 11, the simulation results for this system are shown. In the top figure, the step response is shown using the three different controllers, where a significant reduction in overshoot for both the SPANI and the F-SPANI is observed when compared to the linear controller. Although the main objective of the filters is to reduce the overshoot, the settling time can be of interest as well. In Table I, the settling times are listed, where we take the settling time as the moment when the response no longer leaves a 10% bound around the reference trajectory. The middle graph in Fig. 11 shows the control effort of the (nonlinear) integrator u_s, in which the SPANI and F-SPANI show switching behavior. It can be seen that the SPANI switches slightly after the step response crosses $y = 1$, whereas the F-SPANI switches before $y = 1$. This shows

Authorized licensed use limited to: Eindhoven University of Technology. Downloaded on May 02,2021 at 14:18:11 UTC from IEEE Xplore. Restrictions apply.

This article has been accepted for inclusion in a future issue of this journal. Content is final as presented, with the exception of pagination.

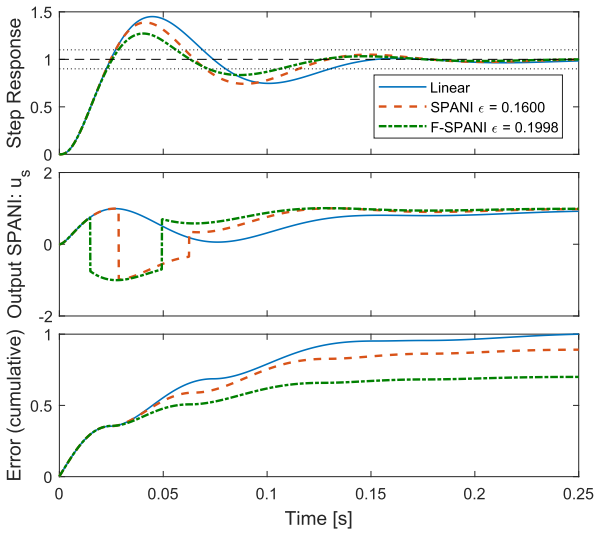

Fig. 11. Simulation results.

that the F-SPANI indeed anticipates the moment at which the error crosses zero, therewith starts to empty the integral buffer sooner, and decreases overshoot. The bottom graph shows the normalized cumulative error over time, i.e.

$$e_{\text{cum}}(t) = \int_0^t |e(\tau)| d\tau. \tag{58}$$

It is observed that the F-SPANI has 27% overshoot, which is a 40% reduction compared to the 45% overshoot of the linear controller. Similarly, the SPANI, with 39% overshoot, has a 13.3% reduction compared to the linear controller. The total cumulative error reduction of the F-SPANI is 30%, compared to a cumulative error reduction of the SPANI of 10.9%, both relative to the performance of the linear controller. In the simulation, of which the results are shown in Fig. 11, the values for ϵ have been reduced to 0.1600 and 0.1998 by fine-tuning. As can be seen in this figure, the reduction of ϵ by 15% has not resulted in oscillations in steady state. In Table I, a comparison is made between the performance of these three controllers, also in terms of the cumulative errors and the settling time. It can be seen that we do not only improve the transient performance in terms of overshoot using the F-SPANI but also decrease the settling time by 17% compared to the linear controller. This improvement in the settling time can be attributed to the fact that due to the reduced overshoot, the system's response can lie within the 10% bound of the reference trajectory earlier. Nonetheless, it is important to note that the rationale behind the design of the F-SPANI is motivated by improving the transient performance in terms of overshoot and, in general, it is not possible to provide guarantees on performance enhancements regarding settling time.

IV. Experimental Results

In this section, we present experimental results on an industrial pick-and-place machine shown in Fig. 12, called the "Hybrid[2]" [31], to validate the different methods in terms of the transient performance improvement. In Section IV-A, a description of the industrial system is provided, followed by a description of the controller selection and design components as well as the measurement results in Section IV-B. Due to company confidentiality, all axes in the figures, and values in the tables, have been scaled.

TABLE I

Performance Overview of the Simulation in Terms of Overshoot, Settling Time, and Cumulative Absolute Error

Controller	Overshoot	Cum. Error	Settling time
Linear	45%	100.00%	0.1303s
SPANI	39%	89.10%	0.1151s
F-SPANI	27%	69.99%	0.1061s

Fig. 12. K&S "Hybrid" with three pick-and-place units.

A. System Description and Industrial Context

The experiments for this article have been performed on the "Hybrid" of Kulicke & Soffa (K&S), as shown in Fig. 12. The machine is used for highly accurate and high-speed pick-and-place operations in chip-manufacturing applications. The "Hybrid" can place up to 33 components per second with an accuracy of up to 7 μm. These components are placed by several parallel pick-and-place units to place multiple components at the same time.

Each unit within the "Hybrid" performs a single pick, single place operation, enabling full control of the process. Multiple units are used in parallel, while the carrier for the components moves between the units. Using this setup, only two degrees of freedom are required for each unit, i.e., the y and z motions as indicated in the schematic representation of a pick-and-place unit in Fig. 13, where the component is picked up in step 1, moved up in z-direction in step 2, moved in y-direction in step 3, and placed in z-direction in step 4.

To achieve the high-accuracy and high-speed placement of components, according to the specifications mentioned above, the transient performance is subject to a switch requirement.

[2]Hybrid is the name of the machine on which experiments are performed and should not be confused with the terminology "hybrid systems".

Authorized licensed use limited to: Eindhoven University of Technology. Downloaded on May 02,2021 at 14:18:11 UTC from IEEE Xplore. Restrictions apply.

This article has been accepted for inclusion in a future issue of this journal. Content is final as presented, with the exception of pagination.

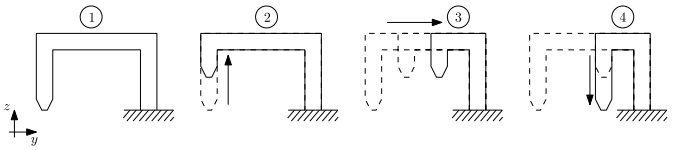

Fig. 13. Schematic of a single pick-and-place unit.

Namely, a component can only be placed (with sufficient accuracy) after the positioning error in the y-direction in step 3 has entered a specified error band. In that sense, transient performance is directly related to the achievable machine throughput capacity.

B. Controller Design and Measurement Results

In the experiments, the y movement of a single pick-and-place unit is used, resulting in a single-input–single-output motion system.

Remark 5: Due to company confidentiality, all values have been scaled, e.g., the overshoot in Table II is scaled to be 50% for the linear controller, and the F-SPANI and SPANI have been scaled accordingly. Also, the time axis in the figures has been scaled. Moreover, the exact values for control settings are company confidential and thus are not specified in this article.

The first step in the design and implementation of the controllers is to construct a model of the system dynamics through basic frequency response function (FRF) measurements (see [30]). Using the measured nonparametric model of the system, a simplified parametric model of a fourth-order system has been fitted to the data, resulting in the Bode diagram in Fig. 14. Such a parametric model is required for carrying out simulations as well as performing stability analysis using Theorem 1 leading to the value for ϵ, which guarantees closed-loop stability.

The plant is currently controlled in a closed-loop configuration similar to the one shown Fig. 1. In the case of linear control, a proportional–integral–derivative (PID)-type controller is used where $\mathcal{C}_{\text{nom}}$ consists of a PD controller and is interconnected in parallel with an integrator with parameter ω_i. In addition, $\mathcal{L}$ and $\mathcal{N}$ are second-order low-pass and notch filters, respectively, utilized for attaining sufficient noise rejection as well as suppression of lightly damped resonance peaks. Moreover, as common in industrial motion controllers, acceleration feedforward with gain m representing the estimated plant mass is used to compensate for the low-frequent rigid-body behavior of the plant dynamics. This describes the current linear control setup as used in the industry. A schematic of the closed-loop system where the linear integrator has been replaced by the F-SPANI is shown in Fig. 15. Note that in Fig. 15, the integrator parameter ω_i is selected to have the same value as used in the linear design. In addition, $\mathcal{C}_f$ is a first-order lead filter, designed to provide phase lead around the closed-loop bandwidth of the system. The addition of $\mathcal{C}_f$ enables F-SPANI to improve transient performance beyond improvements obtained by the SPANI, as we will show in the remainder of this section.

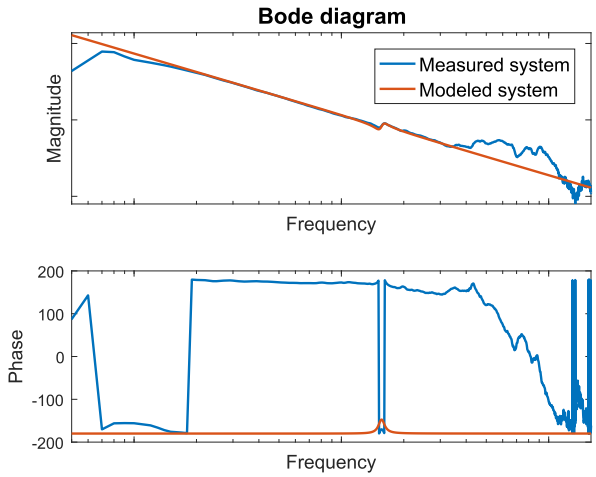

Fig. 14. Bode diagram of the K&S Hybrid. Blue line: measured FRF. Red line: simple parametric model.

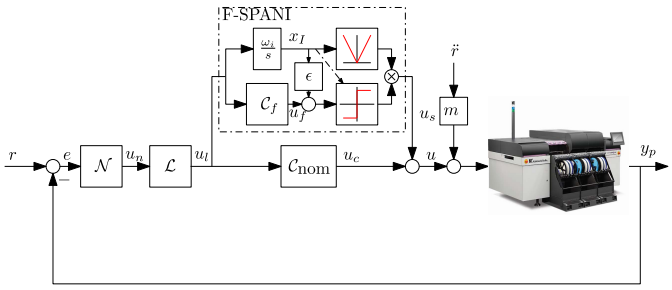

Fig. 15. Schematic of the closed-loop system including the F-SPANI.

Using the parametric model of the plant together with the stability result in Theorem 1, the smallest value for ϵ that would guarantee closed-loop stability has been found to be 0.2075 for the SPANI and 0.2157 for the F-SPANI. As explained in Remark 3, these bounds on ϵ are conservative and can be lowered using manual tuning so that further improvements in transient performance can be obtained. As such, the values $\epsilon = 0.12$ and $\epsilon = 0.15$ have been selected for the SPANI and F-SPANI, respectively, while maintaining a stable response and without introducing undesired oscillations in steady state, under normal operating conditions. Lowering ϵ further all the way to $\epsilon = 0$ results in the closed-loop system tracking the reference trajectory as well; however, the unobservable internal signal u_s will switch rapidly. These fast oscillations are typically undesired in a control system. As such, the parameter ϵ is set at $\epsilon = 0.12$ and $\epsilon = 0.15$. Note that in this particular application, since the stability analysis is slightly conservative, fine-tuning is possible to decrease the parameter ϵ. However, in other industries such as ones involving safety-critical or uncertain systems where robustness and stability guarantees are required (and possibly guaranteed), one should use ϵ-values that satisfy the conditions in Theorem 1 (or use other methods) such that GES of the closed-loop system is guaranteed.

In Fig. 16, the measurement results are shown for five repetitions of the movement to a constant reference position, which is not visible, proving excellent reproducibility. It can

Authorized licensed use limited to: Eindhoven University of Technology. Downloaded on May 02,2021 at 14:18:11 UTC from IEEE Xplore. Restrictions apply.

This article has been accepted for inclusion in a future issue of this journal. Content is final as presented, with the exception of pagination.

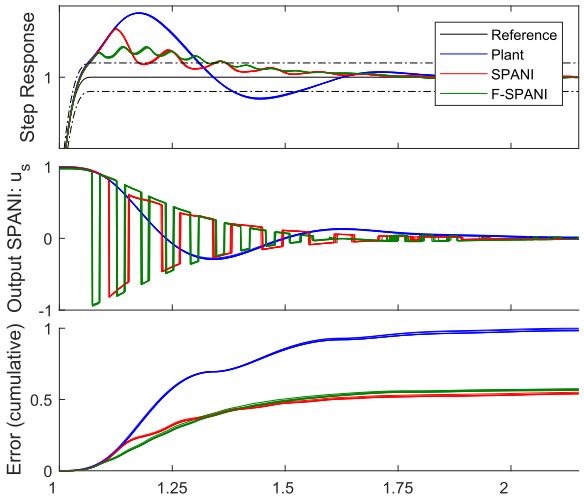

Fig. 16. Measurement results.

TABLE II
MEASUREMENT RESULTS

Controller	Overshoot	Cum. Error	Settling time
Linear	50%	100%	1.53
SPANI	37.66%	54.90%	1.37
F-SPANI	23.59%	57.61%	1.37

be observed that the SPANI and the F-SPANI indeed have significantly less overshoot than the linear controller. Some oscillations are present in the responses of the nonlinear filters, which can be attributed to the fact that the switches in the control action excite some higher order dynamics in the system, which are either not modeled or not captured by the default feedback controller. In this article, the choice is made not to retune the original controller; however, using a redesign of the linear controller, better performance might be obtained for all three controllers. In terms of settling time, the SPANI and the F-SPANI have approximately the same performance, which is 10% better than the linear controller. However, in terms of overshoot, the F-SPANI shows significantly better results than the SPANI. The dashed–dotted lines in the top figure indicate the performance error band used to define settling time. The SPANI and the F-SPANI have approximately the same cumulative absolute error. In Table II, the performance characteristics are summarized for each of the controllers.

V. CONCLUSION AND RECOMMENDATIONS

In this article, a new hybrid integral controller called F-SPANI is introduced to reduce overshoot and thereby improve the transient performance of motion systems while rejecting (low-frequency) disturbances using integral control. The controller is inspired by the SPAN and the SPANI filters; however, it is capable of achieving significantly better transient performance than these existing filters. We presented an LMI-based stability result, which guarantees the stability of the closed-loop system on the basis of a CQLF. In addition, an intuitive describing function analysis is provided to give insight into the rationale and working principle of the F-SPANI. A numerical example has been presented, which shows the potential of the F-SPANI (and existing special cases). The method has been tested on an industrial benchmark system, being a pick-and-place machine, which shows the effectiveness and potential of the proposed approach in an industrial high-tech context. Future work includes the extension of the stability result in Theorem 1 such that less conservative criteria are obtained by, e.g., considering more flexible Lyapunov functions such as piecewise quadratic ones.

ACKNOWLEDGMENT

The authors would like to thank Rik van der Burg and Seyfi Cagil Mayda, Kulicke & Soffa (K&S), for all their support with the experiments.

REFERENCES

[1] M. Seron, J. Braslavsky, and G. Goodwin, *Fundamental Limitations in Filtering and Control*. Berlin, Germany: Springer, 1997.
[2] J. Freudenberg, R. Middleton, and A. Stefanpoulou, "A survey of inherent design limitations," in *Proc. Amer. Control Conf.*, vol. 5, 2000, pp. 2987–3001.
[3] G. F. Franklin, J. D. Powell, and A. Emami-Naeini, *Feedback Control of Dynamic Systems*, 5th ed. Upper Saddle River, NJ, USA: Pearson, 2006.
[4] A. Feuer, G. C. Goodwin, and M. Salgado, "Potential benefits of hybrid control for linear time invariant plants," in *Proc. Amer. Control Conf.*, 1997, pp. 2790–2794.
[5] J. C. Clegg, "A nonlinear integrator for servomechanisms," *Trans. Amer. Inst. Electr. Eng., II, Appl. Ind.*, vol. 77, no. 1, pp. 41–42, 1958.
[6] W. H. T. M. Aangenent, G. Witvoet, W. P. M. H. Heemels, M. J. G. van de Molengraft, and M. Steinbuch, "Performance analysis of reset control systems," *Int. J. Robust Nonlinear Control*, vol. 20, no. 11, pp. 1213–1233, Jul. 2010.
[7] S. J. L. M. van Loon, K. G. J. Gruntjens, M. F. Heertjes, N. van de Wouw, and W. P. M. H. Heemels, "Frequency-domain tools for stability analysis of reset control systems," *Automatica*, vol. 82, pp. 101–108, Aug. 2017.
[8] D. Nešić, A. R. Teel, and L. Zaccarian, "Stability and performance of SISO control systems with first-order reset elements," *IEEE Trans. Autom. Control*, vol. 56, no. 11, pp. 2567–2582, Nov. 2011.
[9] Y. Zheng, Y. Chait, C. V. Hollot, M. Steinbuch, and M. Norg, "Experimental demonstration of reset control design," *Control Eng. Pract.*, vol. 8, no. 2, pp. 113–120, Feb. 2000.
[10] B. G. B. Hunnekens, N. van de Wouw, and D. Nešić, "Overcoming a fundamental time-domain performance limitation by nonlinear control," *Automatica*, vol. 67, pp. 277–281, May 2016.
[11] B. Hunnekens, N. van de Wouw, M. Heertjes, and H. Nijmeijer, "Synthesis of variable gain integral controllers for linear motion systems," *IEEE Trans. Control Syst. Technol.*, vol. 23, no. 1, pp. 139–149, Jan. 2015.
[12] M. F. Heertjes and Y. Vardar, "Self-tuning in sliding mode control of high-precision motion systems," in *Proc. 6th IFAC Symp. Mechatronics Syst.*, Hangzhou, China, 2013, pp. 13–19.
[13] B. Sharif, M. F. Heertjes, and W. P. M. H. Heemels, "Extended projected dynamical systems with applications to hybrid integrator-gain systems," in *Proc. IEEE 58th Conf. Decis. Control (CDC)*, Nice, France, Dec. 2019, pp. 5773–5778.
[14] D. A. Deenen, M. F. Heertjes, W. P. M. H. Heemels, and H. Nijmeijer, "Hybrid integrator design for enhanced tracking in motion control (invited paper)," in *Proc. Amer. Control Conf.*, Seattle, WA, USA, May 2017, pp. 2863–2868.
[15] W. C. Foster, D. L. Gieseking, and W. K. Waymeyer, "A nonlinear filter for independent gain and phase (with applications)," *Trans. ASME J. Basic Eng.*, vol. 88, no. 2, pp. 457–462, Jun. 1966.
[16] S. J. L. M. van Loon, B. G. B. Hunnekens, W. P. M. H. Heemels, N. van de Wouw, and H. Nijmeijer, "Split-path nonlinear integral control for transient performance improvement," *Automatica*, vol. 66, pp. 262–270, Apr. 2016.
[17] A. van der Maas, N. van de Wouw, and W. Heemels, "Filtered split-path nonlinear integrator (F-SPANI) for improved transient performance," in *Proc. Amer. Control Conf.*, Seattle, WA, USA, 2017, pp. 3500–3505.

Authorized licensed use limited to: Eindhoven University of Technology. Downloaded on May 02,2021 at 14:18:11 UTC from IEEE Xplore. Restrictions apply.

This article has been accepted for inclusion in a future issue of this journal. Content is final as presented, with the exception of pagination.

[18] A. Filippov, *Differential Equations With Discontinuous Righthand Sides* (Mathemtaics and its Applications). Dordrecht, The Netherlands: Kluwer, 1988.
[19] R. G. Sanfelice, R. Goebel, and A. R. Teel, "Generalized solutions to hybrid dynamical systems," *ESAIM, Control, Optim. Calculus Variat.*, vol. 14, no. 4, pp. 699–724, Oct. 2008.
[20] J. Aubin and A. Cellina, *Differential Inclusions: Set-Valued Maps and Viability Theory*. Berlin, Germany: Springer-Verlag, 1984.
[21] R. Goebel, R. G. Sanfelice, and A. R. Teel, *Hybrid Dynamical Systems: Modeling, Stability, and Robustness*. Princeton, NJ, USA: Princeton Univ. Press, 2012.
[22] D. Liberzon, *Switching in Systems and Control*. Boston, MA, USA: Springer, 2003.
[23] D. Liberzon and A. S. Morse, "Basic problems in stability and design of switched systems," *IEEE Control Syst.*, vol. 19, no. 5, pp. 59–70, Oct. 1999.
[24] R. A. Decarlo, M. S. Branicky, S. Pettersson, and B. Lennartson, "Perspectives and results on the stability and stabilizability of hybrid systems," *Proc. IEEE*, vol. 88, no. 7, pp. 1069–1082, Jul. 2000.
[25] R. Shorten, F. Wirth, O. Mason, K. Wulff, and C. King, "Stability criteria for switched and hybrid systems," *SIAM Rev.*, vol. 49, no. 4, pp. 545–592, Jan. 2007.
[26] H. Lin and P. J. Antsaklis, "Stability and stabilizability of switched linear systems: A survey of recent results," *IEEE Trans. Autom. Control*, vol. 54, no. 2, pp. 308–322, Feb. 2009.
[27] W. P. M. H. Heemels, B. De Schutter, J. Lunze, and M. Lazar, "Stability analysis and controller synthesis for hybrid dynamical systems," *Philos. Trans. Roy. Soc. London A, Math. Phys. Sci.*, vol. 368, no. 1930, pp. 4937–4960, 2010.
[28] M. T. Heath, *Scientific Computing: An Introductory Survey*, 2nd ed. Singapore: McGraw-Hill, 2005.
[29] H. K. Khalil, *Nonlinear Systems*, 3rd ed. Upper Saddle River, NJ, USA: Prentice-Hall, 2002.
[30] R. Pintelon and J. Schoukens, *System Identification*. Hoboken, NJ, USA: Wiley, 2012.
[31] *K & S HYBRID*, K&S, Singapore, 2017.

B. Sharif received the M.Sc. degree *(cum laude)* in electrical engineering with specialization in systems and control from the Eindhoven University of Technology (TU/e), Eindhoven, The Netherlands, in 2018, where he is currently pursuing the Ph.D. degree with the Control Systems Technology Group, Department of Mechanical Engineering.

His current research interests include hybrid systems and control with a particular focus on formalization, analysis, and design/synthesis of hybrid control solutions aiming at realizing performance beyond limitations of linear time-invariant (LTI) control.

A. van der Maas received the bachelor's degree in biomedical engineering from the Eindhoven University of Technology, Eindhoven, The Netherlands, and the master's degree *(cum laude)* from the Control Systems Technology Group, Department of Mechanical Engineering, Eindhoven University of Technology.

She is currently a Senior Design Engineer with ASML, Eindhoven, working on all mechatronics aspects of the mirror modules in the optical light path of wafer scanners.

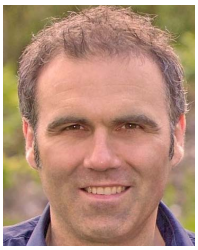

N. van de Wouw (Fellow, IEEE) was born in 1970. He received the M.Sc. degree (Hons.) and the Ph.D. degree in mechanical engineering from the Eindhoven University of Technology, Eindhoven, The Netherlands, in 1994 and 1999, respectively.

In 2000, he was with Philips Applied Technologies, Eindhoven. In 2001, he was with the Netherlands Organisation for Applied Scientific Research (TNO), Delft, The Netherlands. He has held positions as a Visiting Professor at the University of California at Santa Barbara, Santa Barbara, CA, USA, from 2006 to 2007; the University of Melbourne, Melbourne, VIC, Australia, from 2009 to 2010; and the University of Minnesota from 2012 to 2013. He has held a (part-time) full professor position at the Delft University of Technology, Delft, from 2015 to 2019. He is currently a Full Professor with the Mechanical Engineering Department, Eindhoven University of Technology. He is also an Adjunct Full Professor with the University of Minnesota, Minneapolis, MN, USA. He has published the books *Uniform Output Regulation of Nonlinear Systems: A convergent Dynamics Approach* with A. V. Pavlov and H. Nijmeijer (Birkhauser, 2005) and *Stability and Convergence of Mechanical Systems with Unilateral Constraints* with R. I. Leine (Springer-Verlag, 2008). His current research interests include modeling, model reduction, and analysis and control of nonlinear/hybrid and delay systems, with applications to autonomous and cooperative driving, high-tech systems, resource exploration, smart energy systems, and networked control systems.

Dr. van de Wouw received the IEEE Control Systems Technology Award for the development and application of variable-gain control techniques for high-performance motion systems in 2015. He is also an Associate Editor of *Automatica* and the IEEE TRANSACTIONS ON CONTROL SYSTEMS TECHNOLOGY.

W. P. M. H. Heemels (Fellow, IEEE) received the M.Sc. degree *(summa cum laude)* in mathematics and the Ph.D. degree *(summa cum laude)* in control theory from the Eindhoven University of Technology (TU/e), Eindhoven, The Netherlands, in 1995 and 1999, respectively.

From 2000 to 2004, he was with the Electrical Engineering Department, TU/e, as an Assistant Professor. From 2004 to 2006, he was with the Embedded Systems Institute (ESI), Eindhoven, as a Research Fellow. In 2004, he worked at Océ, Venlo, The Netherlands. Since 2006, he has been with the Department of Mechanical Engineering, TU/e, where he is currently a Full Professor. He held visiting professor positions at the Swiss Federal Institute of Technology (ETH), Zürich, Switzerland, in 2001; the University of California at Santa Barbara, Santa Barbara, CA, USA, in 2008; and the University of Lorraine, Nancy, France, in 2020. His current research interests include hybrid and cyber-physical systems, networked and event-triggered control systems, and constrained systems, including model predictive control.

Dr. Heemels was elected as a member of the IEEE-CSS Board of Governors for the term 2021–2023. He was a recipient of a personal VICI grant awarded by NWO (Dutch Research Council). He was a recipient of the 2019 IEEE L-CSS Outstanding Paper Award. He served/serves on the Editorial Board of *Automatica*, *Nonlinear Analysis: Hybrid Systems*, *Annual Reviews in Control*, and the IEEE TRANSACTIONS ON AUTOMATIC CONTROL. He is also the Chair of the IFAC Technical Committee on Networked Systems for the term 2017–2023.

Authorized licensed use limited to: Eindhoven University of Technology. Downloaded on May 02,2021 at 14:18:11 UTC from IEEE Xplore. Restrictions apply.